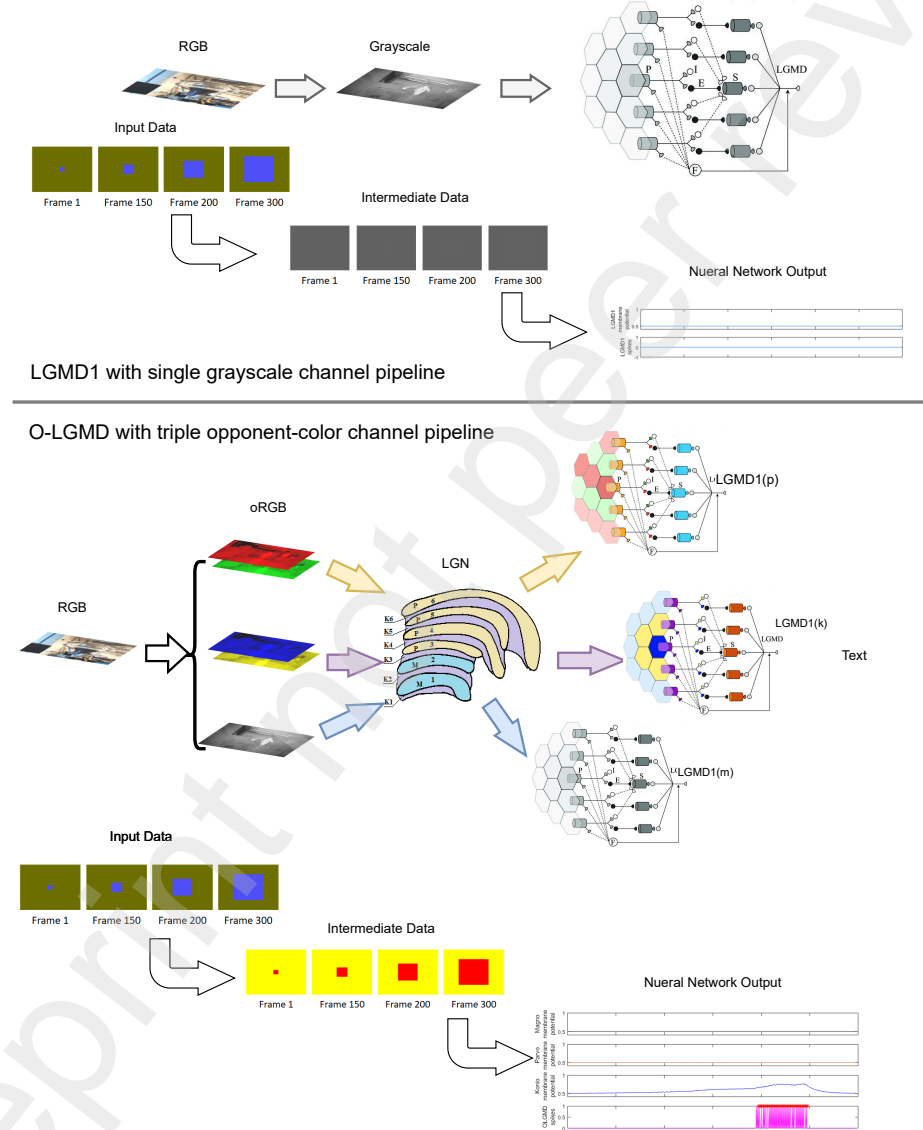


# Graphical Abstract

## An Opponent Colour LGMD Neural Network for Collision Detection at Night with Thermal Camera

Yicheng Zhang, Huizi Han, Hao Luan, Mu Hua, Mei Liu, Heriberto Cuayahuitl, Shigang Yue



## Highlights

### **An Opponent Colour LGMD Neural Network for Collision Detection at Night with Thermal Camera**

Yicheng Zhang, Huizi Han, Hao Luan, Mu Hua, Mei Liu, Heriberto Cuayahuitl, Shigang Yue

- We feed temperature maps to locust-inspired LGMD visual neural networks for night collision detection
- We propose a triple-channel LGMD neural network for collision detection using chromatic colour data
- We have done systematic experiments demonstrating that the proposed OLGMD could detect collision reliably and early at night with thermal data inputs

# An Opponent Colour LGMD Neural Network for Collision Detection at Night with Thermal Camera

Yicheng Zhang<sup>a,b</sup>, Huizi Han<sup>c</sup>, Hao Luan<sup>d</sup>, Mu Hua<sup>b</sup>, Mei Liu<sup>a</sup>, Heriberto Cuayahuitl<sup>b</sup>, Shigang Yue<sup>b,e,\*</sup>

<sup>a</sup>*School of Automation, Guangdong University of Petrochemical Technology, 139, Guanduer Road, Maoming, 525000, Guangdong, China*

<sup>b</sup>*School of Computer Science, University of Lincoln, Brayford pool, Lincoln, LN6 7TS, UK*

<sup>c</sup>*Faculty of Engineering, The Hong Kong Polytechnic University, 11, Yuk Choi Road, Honkong, 999077, China*

<sup>d</sup>*School of Computer Science, Tianjin University of Technology and Education, No.1310, Dagu South Road, Hexi District, 300222, Tianjin, China*

<sup>e</sup>*School of Computing and Mathematical Sciences, University of Leicester, University Road, Leicester, LE1 7RH, UK*

---

## Abstract

It is an enormous challenge for intelligent robots or vehicles to detect and avoid collisions at night because of poor light conditions. Thermal cameras capture the night scenes with temperature maps, often showing in different pseudo-colour modes to enhance the visual effects for the human eyes. Since the features of approaching objects could have been well enhanced in the pseudo colour outputs of a thermal camera, colour cues could likely help the collision detector - lobula giant movement detector (LGMD) to pick up the collision cues nicely. However, no investigation has been published on this aspect, and it is unclear whether the LGMD-like visual neural networks can take pseudo-colour information as inputs for collision detection in extremely dim conditions. In this study, we proposed a model consisting of three sub-networks, each dealing with one specific opponent colour channel, i.e., black-white, red-green, and yellow-blue. A collision alarm will be triggered if any channel's output has exceeded its threshold for a few successive frames. Systematical experiments have been carried out to verify the proposed neural network with different thermal pseudo-colour modes in various

---

\*Corresponding author. E-mail: yueshigang@hotmail.com

nighttime scenarios. Our experiments demonstrated that the proposed bio-inspired collision detection system works well in detecting colliding objects in direct collision courses at low light conditions quickly. The proposed method showed its potential to be part of the sensor systems for future robots or vehicles at night or in other extreme light conditions to avoid fatal collisions.

*Keywords:* collision detection at night, lobula giant motion detector, opponent colour, thermal images

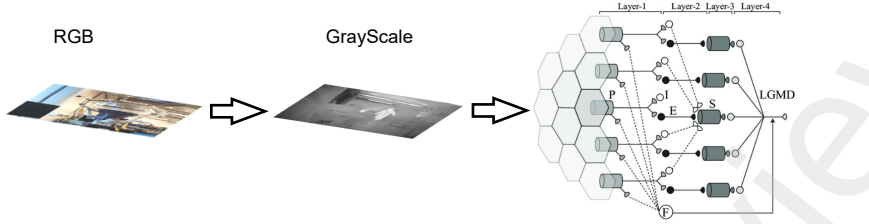
---

## 1. Introduction

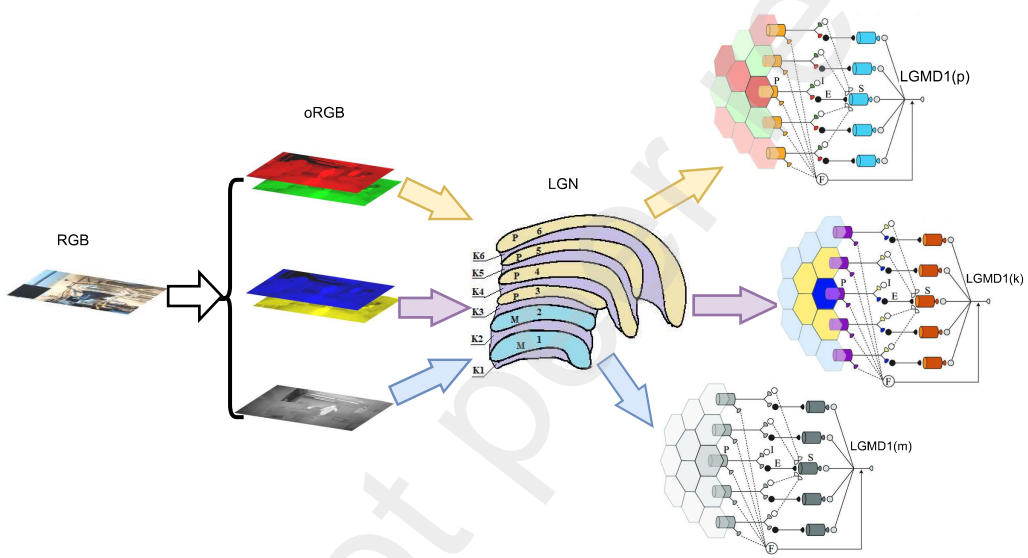
For safety reasons, collision detection is always critical to autonomous ground vehicles (AGV). Vehicle collisions often cause fatalities or serious injuries, exerting huge economic impact on involved individuals. Inspired by the locust's lobula giant movement detector (LGMD) visual neuron, the LGMD-based looming detection methods [1, 2] have robust selectivity for looming cues that lead to imminent collisions and high potential in efficiency and plasticity for realization in low power consumption chips [3]. Therefore, many researchers proposed collision detection and avoidance solutions based on the LGMD neural network in various scenarios, such as unmanned aerial vehicles (UAV) [4–8], robots [9–12], and ground vehicles [13–15].

However, on the one hand, most previous LGMD-based approaches rely on normal visible-light cameras for data collection, focusing more on the first-order perception problem, which is mainly sensitive to luminance changes. When it comes to poor lighting conditions, such as at night or in adverse weather, a regular camera faces considerable challenges in picking up relevant visual cues for collision detection. On the other hand, most of the previous detection processes adopted a monochromatic grayscale pipeline, as shown in Fig. 1(A), and the input data were converted from colour images to grayscale ones before entering the LGMD neural networks. Thus, only the luminance information remains in the postsynaptic network, and the colour cues are lost during this processing. As presented in Fig. 2, the loss of colour information during the conversion from colour to grayscale may lead to the loss of the critical cue, i.e. the expanding edges of a looming object. Therefore, it will be beneficial if colour cues can be well utilized to enhance the looming cues for collision detection.

To compensate for the shortcomings of existing LGMD visual neural networks for collision detection at nighttime, we feed the temperature maps,



(A) Normal pipeline of LGMD based collision detection



(B) Opponent colour LGMD collision detection pipeline

**Fig. 1.** Structure comparison between single channel LGMD1 and O-LGMD. (A) A usual pipeline in the classic lobula giant motion detector(LGMD) model [1]. In this pipeline, colour images are converted into grayscale data, and then they are fed into a four-layer LGMD neural network. (B) The triple-channel opponent-colour LGMD model we proposed. Similar to the three pathways relayed by the Magnocellular, Parvocellular, and Koniocellular layers in the primate's lateral geniculate nucleus (LGN), we decompose the colour image into three sets of opponent colour data: black-white,red-green, and blue-yellow, then send them to LGMD1 for detection respectively.

which are acquired with a long-wave infrared (LWIR) camera at night, to the system. Further, we propose a triple-channel opponent colour LGMD neural network (named O-LGMD) that employs the opponent colour method [16]

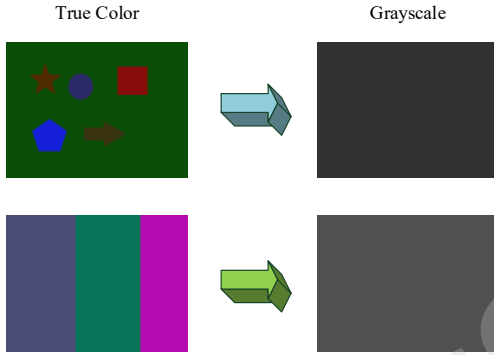


**Fig. 2.** The contour cues vanished after the conversion from colour to grayscale.

inspired by the primates colour vision [17–19] to make full use of the well-enhanced colour information from the thermal camera. This model consists of two main parts. The first part mimics the mechanism from the retina to the lateral geniculate nucleus (LGN) pathways in the old-world monkey’s brain, transforming RGB images into the opponent colour data. The second part is a network of three parallel LGMD neurons responsible for detecting imminent collisions.

The main contributions of this work are summarized as follows: (1) First, we verified that the LGMD-based visual neural network works for collision detection when taking the pseudo-colour thermal images (i.e., temperature maps) as inputs. The thermal inputs are critical for collision detection at night. (2) Secondly, combining the method inspired by mammals’ colour perception pathway with the locust looming motion detector, we proposed a triple-channel O-LGMD visual neural network for night collision detection using pseudo-colour thermal images as inputs. (3) Finally, we systematically test the effectiveness of the new O-LGMD visual neural network via a set of real-world pseudo-colour data from thermal cameras and have approved its capability.

## 2. Related Work

In this section, we summarize the related works in two main areas. In the first subsection, we describe LGMD-related work from biological neurology study to the evolved research carried out using LGMD-based visual neural

networks for collision detection. The second subsection is about opponent colour methods from the biological neurology research of colour vision to the modelling works for image processing.

### *2.1. The LGMD-based collision detection algorithms*

Collision detection benefits a lot from biological neuroscience studies. Early in the 1970s, O’Shea et al. identified the lobula giant movement detector (LGMD) neuron in locusts via anatomical methods [20, 21]. In the mid to late 1990s, the computational models of LGMD were proposed and verified by several research groups. Hatsopoulos and Gabbiani et al. proposed an LGMD looming object detection method by judging the angular threshold and its changing rate [22–24]. At the same time, Rind and Bramwell [1] introduced an LGMD1 computational model from another perspective. This 4-layer feed-forward neural network with lateral inhibition is simple and efficient, making it easy to deploy on single-chip solutions, such as FPGA [25]. Later, Yue and Rind improved the above model into a 5-layer one [2]. With an extra group excitation and decay processing layer, the new LGMD1 model is more robust and adaptive to dynamic backgrounds in robotic experiments. Then, Fu and Yue set up an LGMD2 model with ON/OFF channels after the photo-receptor layer [26]. Although the LGMD2 model is only selective to dark approaching objects against the brighter ground, it mended up some drawbacks of LGMD1, such as better resistance to the disturbance from the changing ambient illumination.

In recent years, LGMD-based methods have demonstrated a diverse development trend. Improved models for solving specific problems have emerged. For UAV applications, Zhao et al. proposed a distributed presynaptic connection-based LGMD1 model(D-LGMD1) [4]. This model uses both spatial and temporal filters in lateral inhibition to retain only the most critical information for collision detection, suppressing translation and minor background movements. Thus, the D-LGMD1 is suitable when the camera body moves at high speed. Lei et al. demonstrated an enhanced LGMD1 model with ON/OFF dual channels [27, 28]. This model effectively inhibits the responses to translation motions by judging the combination results from both pathways. Hua et al. added an extra layer that mimics the neuronal refractoriness to the LGMD1 model [29], making it more robust.

Meanwhile, the proven LGMD models had become part of newly proposed synthetic vision systems. For example, Zhang et al. proposed a neural network integrating LGMD and a direction-selective network (DSN) for col-

lision prediction [30]. By applying different detection neurons to different regions of the visual field, the fusion model is more practical for ground-driving scenarios. Hu and Fu established a visual motion cues discrimination neural network (ViMDNN), which included four motion detection neurons: LGMD1, LGMD2, and two DSNs [31, 32]. In their model, vision cues extracted by different presynaptic neurons are synthesized in the postsynaptic network with lateral inhibition.

## 2.2. *The opponent process in biology and colour models*

The scientific study of colour started in the 17th century [33]. The most well-known two colour vision theories are the Young-Helmholtz theory about trichromatic colours [34, 35] and the Hering theory of the opponent process [36]. With the development of modern biological neuroscience, it is now generally accepted that these two theories describe the different stages of colour perception [37, 38]. From a biological point of view, mammalian eye photoreceptors contain three types of cones sensitive to three different wavelengths of light [39, 40]; the process at this stage is consistent with the trichromatic theory. In the next step, the specific retinal ganglion cells encode colour signals into opponent pairs and successive them to the lateral geniculate nucleus(LGN), which only accepts dichromatic input [41]. Therefore, Herring's opponent colour theory is more suitable for neural networks in the visual pathway.

Colour models are the mathematical representations of related theories. Ibraheem et al. reviewed several of the most common colour models and their characteristics and application areas [42]. Some recent studies have used multiple colour models to complement each other. For example, Dong et al. introduced an RLCM method that uses both red-green-blue (RGB) and International Commission on Illumination (CIE)  $L^*a^*b$  models to enhance underwater images [43]. Their model outperformed the others on two underwater image datasets by using histogram equalization in channels of the RGB model and contrast improvement under the  $L^*a^*b$  model.

New colour models have also been proposed in specific application areas. Yan et al. presented a quantum colour model based on the original hue-saturation lightness model (named QHSL), which can be used in potential quantum computing hardware [44]. Luo et al. set up an LLAB( $l : c$ ) colour model derived from the CIE  $L^*a^*b$  colour space [45]. This model aims to handle the chromatic adaptation problem of colour appearance. To obtain a proper red-green opponent channel, Bratkova et al. established an opponent

colour model (oRGB) [16].

According to their low computational consumption, colour-based methods are widely adopted in recognition of objects known to have relatively fixed colours, such as flames [46, 47], skin [48], fruits [49, 50], and so on. Colour models are also applied in other computer vision tasks, such as image segmentation, object tracking, etc [51–54]. But, to the best of our knowledge, very few motion perception approaches consider colour cues.

### 3. Proposed Method

In the following, we will formulate the proposed opponent colour triple-channel LGMD visual neural network (O-LGMD). As can be seen in Fig. 1(B), the O-LGMD neural network comprises two major functions. One is the opponent colour transformer which transforms the data from the RGB colour space to the oRGB space. Here we named the channels relaying oRGB data by magnocellular(M), parvocellular(P), and koniocellular(K), corresponding to the three layers in the primate’s LGN. The other is the LGMD-based collision detector which consists of three parallel and independent LGMD1 neural networks. Each LGMD1 neuron will be responsible for the detection of one opponent-colour channel.

#### 3.1. The RGB-oRGB Transformation

As stated above, the opponent process occurs from the retina to the LGN pathway within the primate visual system. To mimic the mechanism of the opponent pathway optic nervous system, we convert *RGB* images into *oRGB* data using the method introduced in paper [16].

The opponent colour transformation includes two steps. The first step is a linear colour space conversion from *RGB* to  $LC_1C_2$  using equation 1. The shape of the colour space is changed from a cube to a parallelepiped. In this intermediate linear space, the colours are distributed in a hexagon on a plane perpendicular to the black-white axis. The vertices of the hexagon are blue, magenta, red, yellow, green and cyan.

$$\begin{bmatrix} L \\ C_1 \\ C_2 \end{bmatrix} = \begin{bmatrix} 0.299 & 0.587 & 0.114 \\ 0.500 & 0.500 & -1.000 \\ 0.866 & -0.866 & 0.000 \end{bmatrix} \begin{bmatrix} R \\ G \\ B \end{bmatrix} \quad (1)$$

To obtain a true Hering-style opponent colour space, making the red-green axes and the blue-yellow axes orthogonal, a non-uniform rotation around the

luma axis  $L$  is carried out as the second step:

$$\begin{bmatrix} C_{yb} \\ C_{rg} \end{bmatrix} = \begin{bmatrix} \cos(\theta_0 - \theta) & -\sin(\theta_0 - \theta) \\ \sin(\theta_0 - \theta) & \cos(\theta_0 - \theta) \end{bmatrix} \begin{bmatrix} C_1 \\ C_2 \end{bmatrix} \quad (2)$$

where  $\theta = \text{atan}(C_2, C_1)$  is the original angle in the  $LC_1C_2$  linear chroma plane, and  $\theta_o$  is the final angle after rotation which can be calculated by:

$$\theta_o = \begin{cases} (3/2)\theta & \text{if } \theta < \pi/3 \\ \pi/2 + (3/4)(\theta - \pi/3) & \text{if } \pi \geq \theta \geq \pi/3 \end{cases} \quad (3)$$

Thus, by extending the positive half-plane as well as compressing the negative half-plane of the x-axis, we obtained a colour gamut with Hering-style opponent axes. The final output of the RGB-oRGB conversion is as equation 4:

$$F' = \begin{bmatrix} L \\ C_{yb} \\ C_{rg} \end{bmatrix} \quad (4)$$

where  $L$  contains the luminance data,  $C_{yb}$  and  $C_{rg}$  provide the opponent colour information of the original image.

### 3.2. The LGMD-based Neural Network

To perceive the looming motion in each channel of the opponent colour space, we set up three LGMD1 neural networks with reference from paper [4] and [12]. Each LGMD neuron includes four presynaptic layers and a feed-forward inhibition branch. Below we describe one LGMD neuron as an example.

#### 3.2.1. P layer

Like photoreceptors in facets or retinas, the P cells captured the value of each pixel in the input image. For a colour image with triple opponent colour channels,  $L$  represents luminance in the black-white channel while indicating the chromatic differences in the other two channels.

$$P(x, y, t) = \left| L(x, y, t) - \int L(x, y, s) \delta(t - s - 1) ds \right| \quad (5)$$

where  $P(x, y, t)$  is the change in the value of pixel  $(x, y)$  at time  $t$ ,  $\delta$  indicates the Dirac delta distribution of the historic value. The output of P layer reflects the value difference of each point in the temporal domain. P cells will not be excited when there is no difference between successive frames.

### 3.2.2. EI Layer

Receiving the signal from the P layer, the EI layer possesses a population of excitatory cells and inhibitory cells. The excitatory cells transmit data directly to the S layer, where the output of late-arriving lateral inhibition cells will suppress their value. These processes can be given by:

$$E(x, y, t) = P(x, y, t) \quad (6)$$

$$I(x, y, t) = w_I \otimes P(x, y, t - 1) \quad (7)$$

where  $E(x, y, t)$  and  $I(x, y, t)$  are the output of both excited and inhibited cells at pixel  $(x, y)$  at moment  $t$ ,  $\otimes$  represents the convolution operation. The local inhibition weight  $w_I$  is denoted by:

$$w_I = \begin{bmatrix} 0.125 & 0.25 & 0.125 \\ 0.25 & 0 & 0.25 \\ 0.125 & 0.25 & 0.125 \end{bmatrix} \quad (8)$$

### 3.2.3. S Layer

The S layer sums the output of E cells and I cells by:

$$S(x, y, t) = E(x, y, t) - \alpha I(x, y, t) \quad (9)$$

where  $\alpha$  is a constant representing the global inhibition weight.

### 3.2.4. G Layer and Feed-Forward Inhibition

The G layer will pass those cells surrounded by strong excitations through and filter the isolated excitations simultaneously. The excitation corresponded to cell  $(x, y)$  becomes:

$$G(x, y, t) = S(x, y, t) Ce(x, y, t) \omega^{-1} \quad (10)$$

where  $Ce(x, y, t)$  is the passing coefficient matrix, and  $\omega$  is a scale factor, they can be computed by Eq. 11 and Eq. 12 respectively:

$$Ce(x, y, t) = \iint_{\Omega} S(x, y, t) dx dy \quad (11)$$

where  $\Omega$  is the neighbourhood area which is a  $3 \times 3$  matrix in this model.

$$\omega = \Delta c + \max(|Ce(x, y, t)|) C_W^{-1} \quad (12)$$

where  $C_W$  is a constant,  $\Delta c$  is a small real number which makes sure the denominator in Eq. 9 won't be zero.

To reduce the false-positive results because of the large scale of pixel change during a quick turning, we employed a feed-forward inhibition(FFI) branch before the output of the G layer.

$$\tilde{G}(x, y, t) = \begin{cases} G(x, y, t), & \text{if } C_{de} \cdot G(x, y, t) \geq T_{de}(t) \\ 0, & \text{otherwise.} \end{cases} \quad (13)$$

where  $\tilde{G}(x, y, t)$  is the available output from G layer,  $T_{de}(t)$  denotes an adaptive threshold generated in the FFI pathway that makes the G layer output more reasonable. It is provided by:

$$T_{de}(t) = \frac{\text{FFI}(t)}{n_{cell} \cdot m} \cdot T_0 \quad (14)$$

where  $T_0$  is the initial threshold,  $n_{cell}$  is the total number of pixels in a frame,  $m$  is a coefficient. The FFI( $t$ ) is supplied by:

$$\text{FFI}(t) = \iint |P(x, y, t - 1)| dx dy \quad (15)$$

### 3.2.5. LGMD cell

The LGMD cell accumulates the whole excitatory value in space to generate membrane potential by the following equation:

$$K(t) = \iint |\tilde{G}(x, y, t)| dx dy \quad (16)$$

then normalized by a sigmoid function as below:

$$k(t) = \text{Sigmoid}(K(t) \cdot n_{cell}^{-1}) \quad (17)$$

### 3.2.6. Spiking mechanism

The comparison result between the membrane potential  $k(t)$  and a threshold  $T_{MP}$  fabricates the collision warning spikes:

$$S_{ch}^{\text{spike}} = \begin{cases} 1, & \text{if } k(t) \geq T_{MP} \\ 0, & \text{otherwise.} \end{cases} \quad (18)$$

where  $S_{ch}^{\text{spike}}$  is the spike output by one single LGMD1 neuron network.

Based on the content introduced above, we achieved a single-channel LGMD1 computational model. Note that the proposed O-LGMD model has three independent LGMD1 neural networks. Each will produce a spike when a stimulus in the corresponding channel triggers the depolarization condition. As a result, we chose a simple and effective method by synthesising them via logical OR in this study:

$$S_{final}^{\text{spike}} = \begin{cases} 1, & \text{if } (S_{ch1}^{\text{spike}} | S_{ch2}^{\text{spike}} | S_{ch3}^{\text{spike}}) = 1 \\ 0, & \text{otherwise.} \end{cases} \quad (19)$$

where  $S_{ch1}^{\text{spike}}$ ,  $S_{ch2}^{\text{spike}}$ ,  $S_{ch3}^{\text{spike}}$  correspond to the action potentials in the Magnocellular, Parvocellular, and Koniocellular channels of the O-LGMD model, respectively.

At the last stage, by counting the number of the global spikes in a sliding time window, the final collision warning synapse can be issued by:

$$C_{final}^{\text{LGMD}} = \begin{cases} 1, & \text{if } \sum_{t-n_{ts}}^t S_{final}^{\text{spike}} \geq n_{sp} \\ 0, & \text{otherwise} \end{cases} \quad (20)$$

where  $n_{ts}$  is the size of the sliding time window, and  $n_{sp}$  is the warning signal firing threshold.  $C_{final}^{\text{LGMD}}$  represents the final collision warning synapse, where 1 indicates there is a risk of collision, and 0 means no.

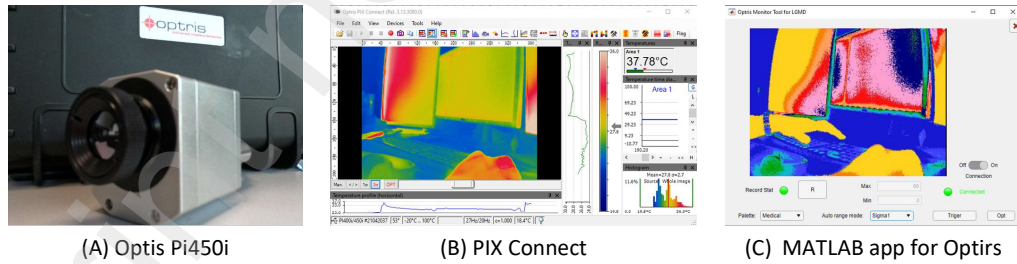


**Fig. 3.** Data collection equipment and software. (A) Opiris Pi 450i long-wave infrared camera; (B) PIX Connect; (C) the thermal video capture MATLAB app we developed.

## 4. Experiments

We conducted two kinds of experiments to verify the effectiveness of the O-LGMD model. In the first type of experiment, we use the synthesized animation as the input data. In these animations, we specified the foreground object colour and the background colour in the different motion scenes to test whether it has the ability of collision recognition like the LGMD1 model and if it can distinguish colours. In the second type of experiment, we employed pseudo-colour videos of real-world collision scenes to validate whether colour cues help improve the looming object detection performance in dimly lit environments with thermal input data.

### 4.1. Experiment Setup

The hardware we used in our experiments includes an Optris Pi450i long-wave infrared (LWIR) camera (Fig. 3(A)) and a desktop PC with a 3.4GHz CPU and 32GB RAM. The software platform is composed of Blender 3.3.1, PIX connect 3.13 (Optris GmbH, Berlin, Germany, as Fig. 3(B)) and MATLAB R2021b (The MathWorks Inc., Natick, USA). We used Blender to generate test animations in the first part of our experiments. The real-world

**Table 1**

The Parameters of the LGMD1 computational model. One set of these parameters is used in the LMGD1 model [12]. The O-LGMD used 3 sets of the same parameters, one set in each channel.

Name	Value	Description
$\alpha$	0.7	inhibition constant in equation 9
$\Delta c$	0.01	coefficient in equation 12
$C_w$	4	factor in equation 12
$C_{de}$	0.5	decay coefficient in equation 13
$T_0$	0.5	initial constant in equation 14
m	0.4	constant in equation 14
$n_{cell}^1$	110016	total pixels of a frame image in equation 14
$T_{MP}$	0.7	the membrane potential threshold in equation 18
$n_{ts}$	4	sliding window size in equation 20
$n_{sp}$	3	firing threshold in equation 20

<sup>1</sup> This value varies according to the physical resolution of the camera

thermal data are captured by an Optris PI 450i. PIX Connect is the thermal video capture software provided by the camera manufacturer; it is very powerful and friendly. However, this software can only output videos in ravi format, which entirely records the thermal raw data but is inconvenient for other programs to access. So, we developed a MATLAB app (Fig. 3(C))for thermal data acquisition based on IRImagerDirect SDK(Evocortex Inc. , NÜremberg,Germany), which can save files in mp4 or avi format. The resolution of the infrared data is  $382 \times 288$  pixels. All the thermal data are captured in 1-sigma temperature scaling mode at 27Hz frame rate. Programs implemented of all bio-inspired models are coded in MATLAB. In the O-LGMD detection model, we use a group of symmetrical parameters; in other words, three LGMD neurons in the different channels are initialized with the same parameters listed in Table 1.

#### *4.2. Motion detection responses test*

To test the basic function of the movement detector, we first generated a set of grayscale animations. In these animations, a solid black square represents the moving object to detect, and the background is white. We then compared the responses of the O-LGMD and the LGMD1 models to three movement stimuli; they are looming, receding, and translating. As demonstrated in Fig. 4, among the three opponent-colour channels, only the magnocellular channel responds to the black-white looming stimulus, and its membrane potential is precisely the same as the output of the LGMD1 model. Fig. 5(A) and Fig. 5(B) are their responses to the receding movement with and without the feed-forward inhibition respectively, and Fig. 5(C) shows the results of translating stimulus responses of the two models. These results reveal that when the input data are grayscale images, the O-LGMD model has the same responses to motions as the previous LGMD1 model[1, 2].

#### *4.3. Opponent colour Response Test*

One of the essential functions of O-LGMD is to pick up colour cues as well as illumination cues in collision detection processing. As stated in the introduction section, some colours that look significantly different may have very similar grayscale values after the conversion. To test whether the O-LGMD model can correctly respond to a typical motion stimulus in this case, we made test animations in the colour pairs that satisfy the above conditions. Fig. 6 and Fig. 7 provide the opponent-colour response result comparison of three LGMD-based models: O-LGMD, LGMD1, and LGMD2. The top line

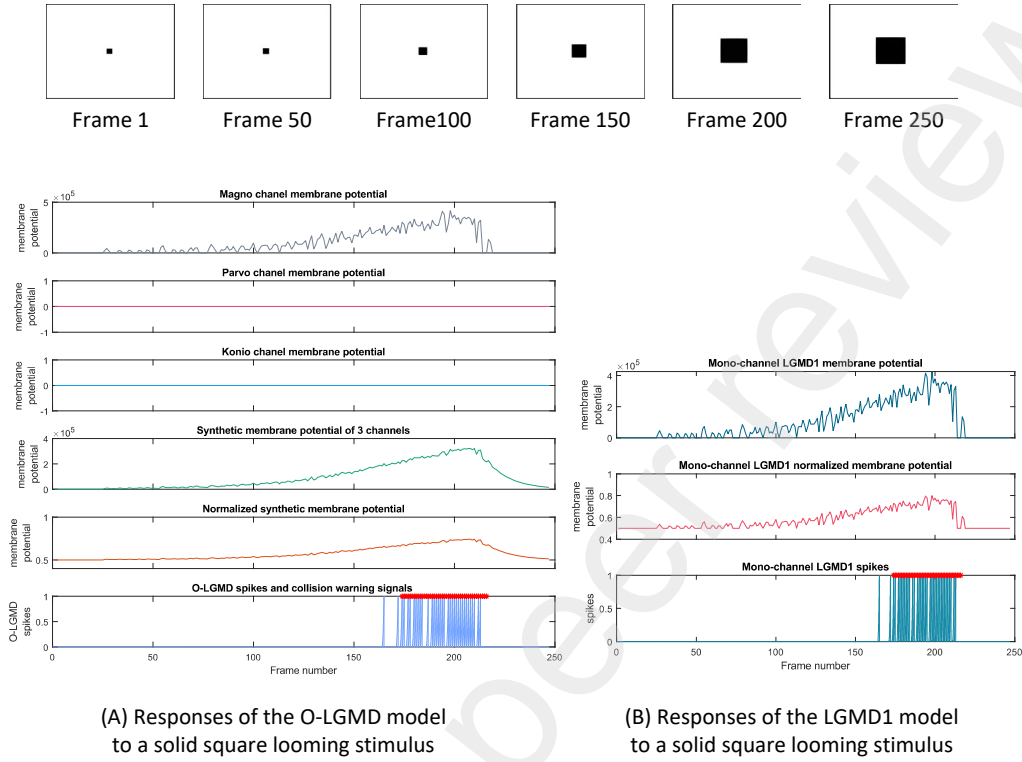


**Fig. 4.** Looming stimulus results in comparison between the O-LGMD and the LGMD1 models. In this animation, a black block is looming on the white background. The top row of images is the frames sampled from our test video. (A) The upper three axes show the response results in the three opponent-colour layers respectively; The fourth axis plots the synthetic result of the above three channels; the fifth graph is the normalized result of the synthetic result, and the bottom one demonstrates the firing spikes(blue peaks) and collision warning signals(red asterisks). (B) Responses of the LGMD1 model to a looming stimulus. The result shows that when the input is a grayscale image, the O-LGMD only responds to the magnocellular layer, which is consistent with the response of the LGMD1.

includes pictures sampled from one of our motion stimulus-response testing animations, and images in the second row from the top are the outputs of their grayscale conversion. By comparing the first and second rows of images, it is easy to tell that the moving object is more salient with colour cues than just luminance cues. As can be seen in the upper three curves, which represent the responses in the three LGN channels of O-LGMD. For

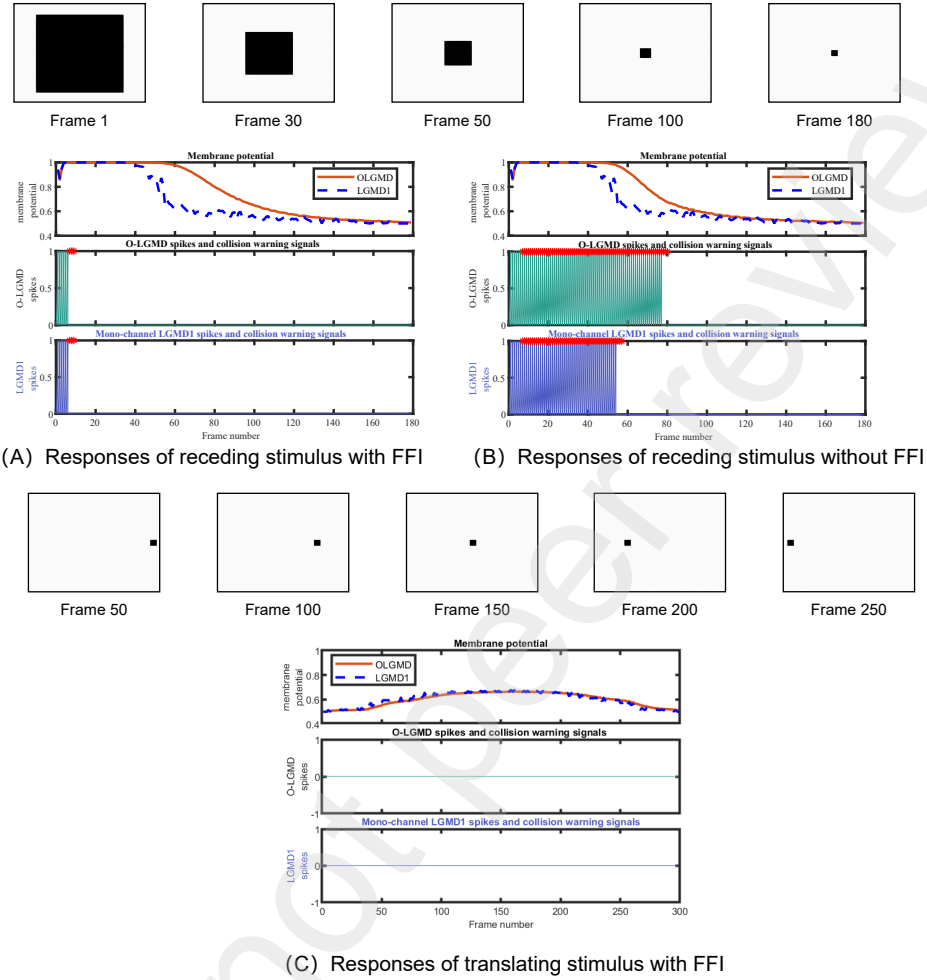


**Fig. 5.** Responses of the O-LGMD and the LGMD1 to receding and translating stimulus. In each sub-figure, the upper axis includes the O-LGMD and the LGMD1 normalized synthetic membrane potentials in a specific stimulus. The middle and the bottom are the spike timing of the two models, respectively. The proposed O-LGMD's responses to receding and translating objects are suppressed by the FFI, similar to the previous LGMD model[1, 2]

the red-green opponent colour looming stimulus (see Fig. 6), the parvocellular channel of the OLGMD model gave correct responses. In the same way, the koniocellular channel responds to the blue-yellow theme looming stimu-

lus (see Fig. 7). As a result, for input with sufficient colour differences, the O-LGMD model can output relatively ideal responses to motion stimuli. On the contrary, the single-channel LGMD1 and LGMD2 models failed to detect collision risks in both situations, for there are not enough illuminance differences in the grayscale images. Similar experiment results delineated that the opponent-colour discrimination ability of the parvocellular channel and the koniocellular channel in the O-LGMD model contribute to collision detection as long as the input data have enough colour differences.

#### 4.4. Real-world Pseudo-colour Thermal Data Test

Although the above results proved the O-LGMD model responds to motion stimuli in both illuminance-changing and colour-difference variants, it is necessary to test its efficiency in real-world scenes further.

In the first step, we compared the detection results of the O-LGMD and the LGMD1 models in nine pseudo-colour palettes. Here we did not add the LGMD2 model to comparisons because we pay more attention to objects with higher temperatures than the environment, such as pedestrians or animals, which are generally brighter in infrared thermal images.

The Optris Pi450i camera supports a total of 11 colour palettes, including two grayscale schemes and nine pseudo-colour modes. As shown in Fig. 8, the same pedestrian approaching scene is captured in nine pseudo-colour themes: red, green, blue, iron-hi, iron, blue-hi, rainbow, rainbow-hi, rainbow-medical. The results of the nine modes are distributed in a nine-square grid in Fig. 8. In each grid, the Upper left is a sample video frame, and the upper right shows the corresponding pseudo-colour palette in a bar, the bar's colour from left to right represents low temperature to high temperature in the thermal image. The three axes below, from top to bottom, illustrate the membrane potential of two models, the O-LGMD's spike firing and the LGMD1's spike firing.

By comparing the looming stimulus-response between LGMD1 and O-LGMD in each pseudo-colour palette, it can be known that when the parameters of the three channels in the O-LGMD neural network are consistent, the O-LGMD responds to movement stimulus earlier than the LGMD1 in the red and blue themes. Two models both gave out a lot of false positive results in the rainbow-medical theme. In the rest of the palettes, there is not much difference between the results of the two models. As mentioned earlier, the O-LGMD neural network is not superior to the LGMD1 in all cases. It can play its role only if the brightness difference is slight after the picture is converted to grayscale and the colour difference is relatively apparent. It

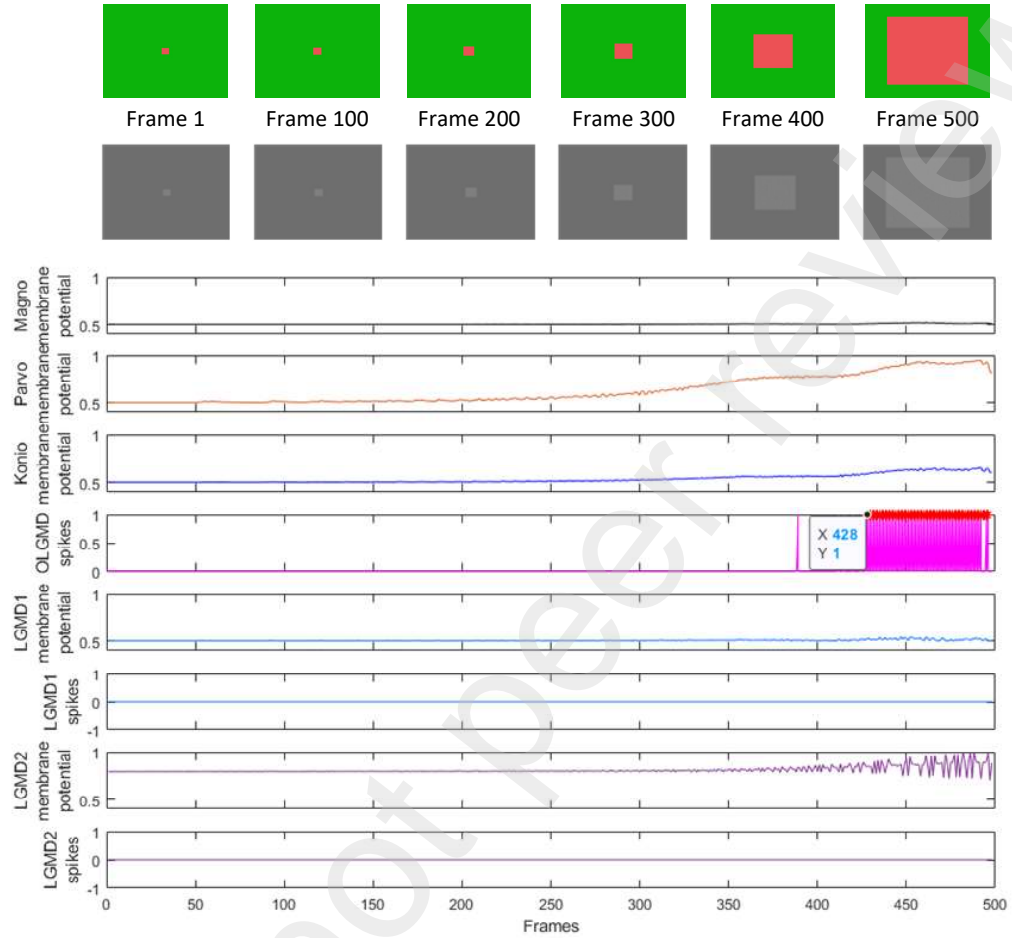


**Fig. 6.** Looming stimulus responses of different LGMD-based models in Red-green opponent colour. In this synthetic animation, a solid red square on a green background approaches the viewer from a distance. The top line of pictures are sample frames of the original animation; Those in the second row are their corresponding grayscale images. Curves from top to bottom demonstrate the membrane potential and the synaptic spikes of the O-LGMD, the LGMD1, and the LGMD2 in the time domain, respectively. If a collision risk is detected, the warning signal issued by the model will be drawn above the spike sequence curve in the form of a red asterisk.

can be seen from the sampling frames in Fig. 8 that in most pseudo-colour palettes, there are significant brightness differences between the target and the background, and only the red and blue monochrome modes meet the

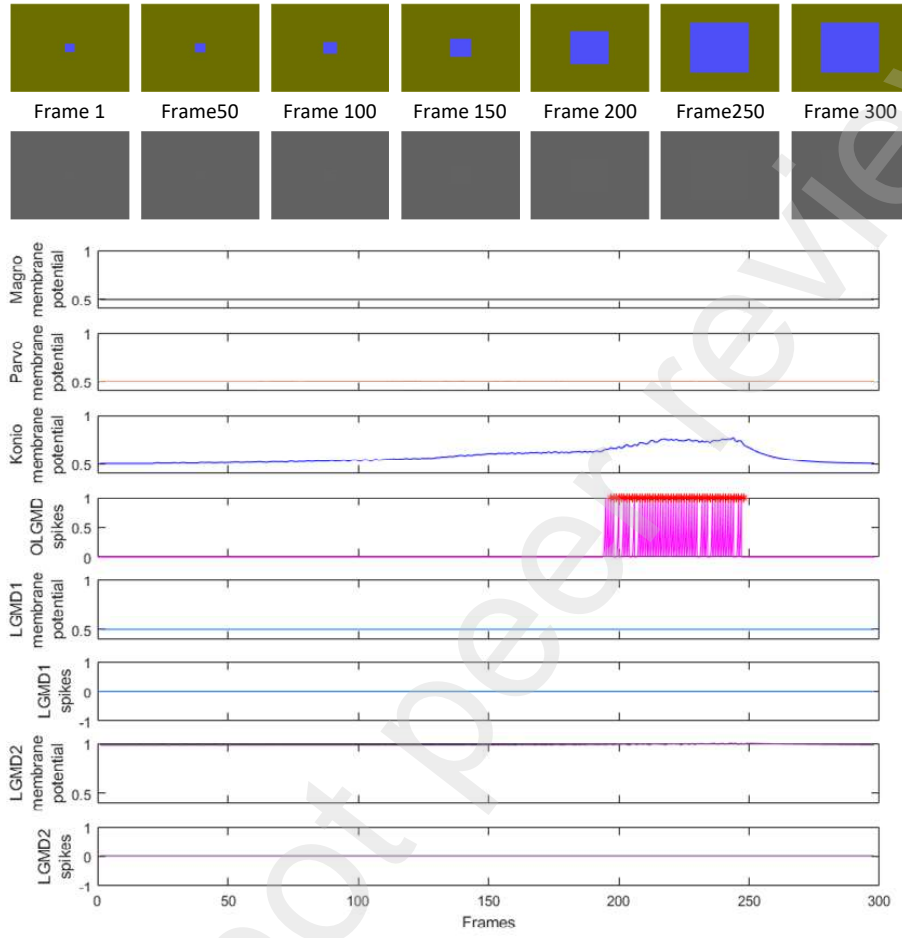


**Fig. 7.** Looming stimulus responses of different LGMD-based models in Blue-yellow opponent colour. A solid blue square on a dark-yellow background is set up in this test. The top row of images are original video sample frames; the second row includes the pictures after being converted into grayscale. Again, depending on the output of the koniocellular layer, the O-LGMD model responded to the looming stimulus correctly. But the LGMD1 and LGMD2 models in the monochromatic pipeline show no responses to the looming stimulation due to the lack of luminance difference.

above conditions.

In the second step, we mainly evaluated the

model's responses to real-world motion stimuli in scenes with red and blue pseudo-colour palettes in extremely low-light environments. Fig. 9 contains two test results in the scene where a 5mm diameter small ball approaches

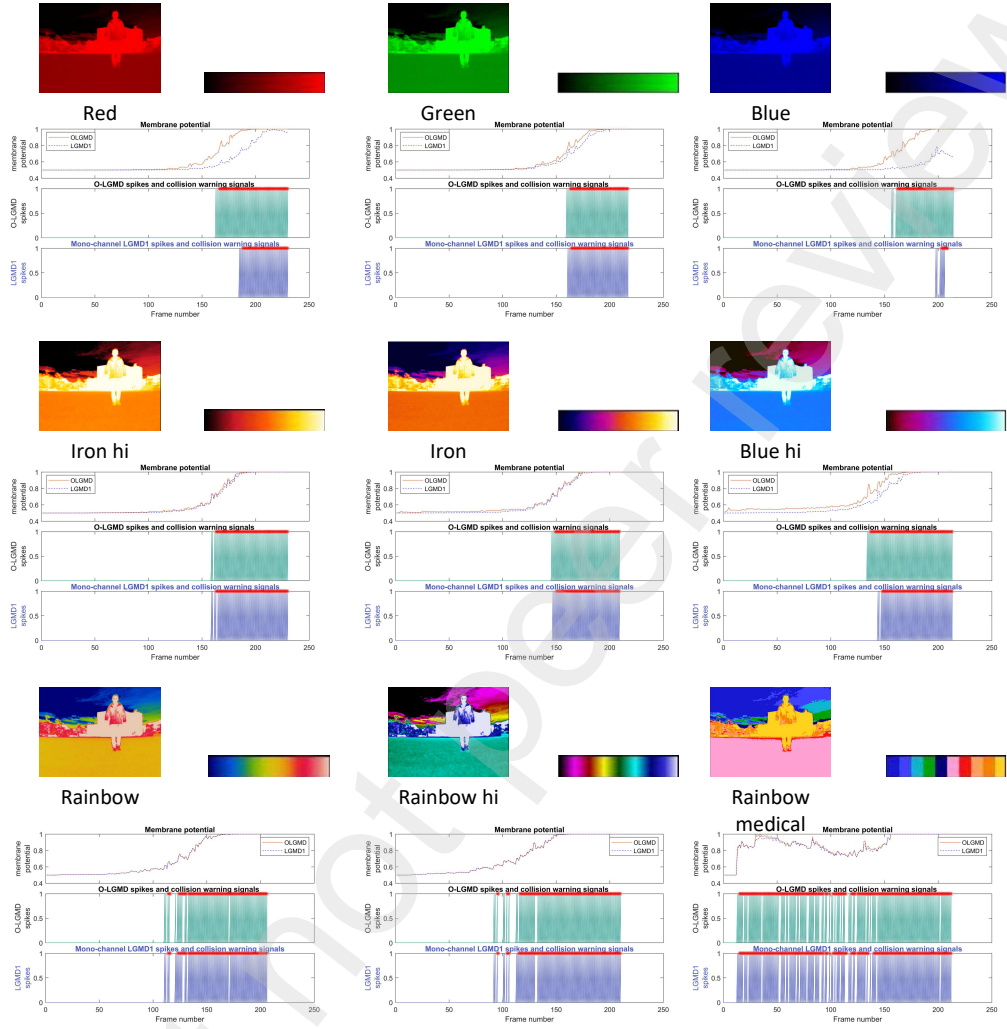
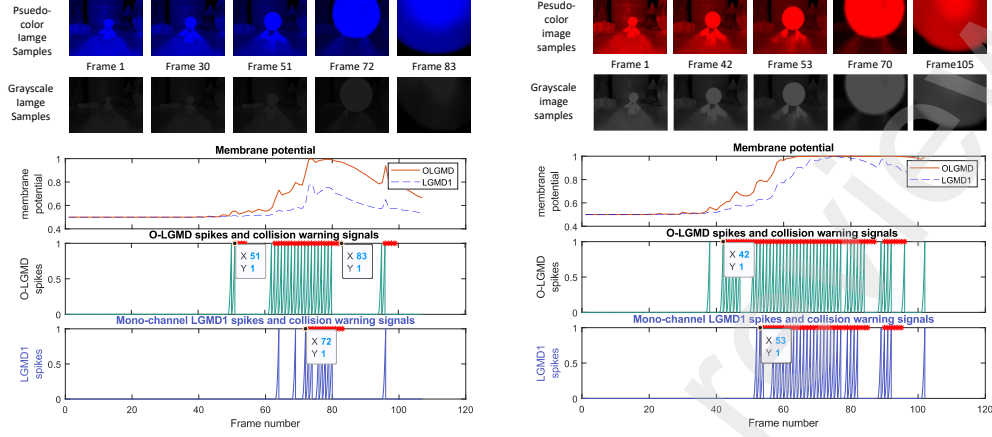


**Fig. 8.** Comparison of the results in different pseudo-colour palettes. When the parameters of the three channels are the same, the performance of the O-LGMD model is better than that of the LGMD1 in blue and red pseudo-colour modes; when other pseudo-colour palettes are used, the difference between the two is little.

the camera along the central axis of the camera. The results of both experiments showed that the membrane potential of the O-LGMD would peak earlier than that in the LGMD1. In the blue palette, as shown in Fig. 9(A),



(A) Looming detection in blue palette      (B) Looming detection in red palette

**Fig. 9.** Responses of the O-LGMD and the LGMD1 to real-world looming stimulus test. The top two lines are test video sample frames and their grayscale conversion results. The lower part of the figure displays the membrane potential of the O-LGMD and the LGMD1 and their spikes firing, respectively.

the O-LGMD fired spikes twenty-one frames earlier than the LGMD1, and in the red theme, as demonstrated in Fig. 9(B), the O-LGMD gave out collision warning signals eleven frames ahead of the LGMD1. These results demonstrate that O-LGMD responds more acutely to looming stimuli in the red or blue pseudo-colour palette in dark environments.

Within the field of view (FOV) of the camera, when the small ball approaches the camera from different angles, for example, the target deviates from the lens axis at 0 degrees, 10 degrees, 20 degrees and 30 degrees, as shown in Fig.14, The responses of O-LGMD are very similar in all these directions. Fig. 10(A) is a schematic diagram of the experimental setup, and Fig. 10(B) shows the normalized synthetic membrane potential curves of the O-LGMD model when responding to the looming stimuli from these directions. By comparing these curves, it is not difficult to see that regardless of the direction from which the stimulus comes, depolarization will occur in the O-LGMD neural network when the object at risk of collision is within a specific range of relative distances.

A group of near-miss trajectories are set up as displayed in Fig. 11(A). From a distance of 1300mm, the 50mm diameter ball moves along axes with 0, 10, 20, and 30 degrees to the central axis of the camera. As revealed by

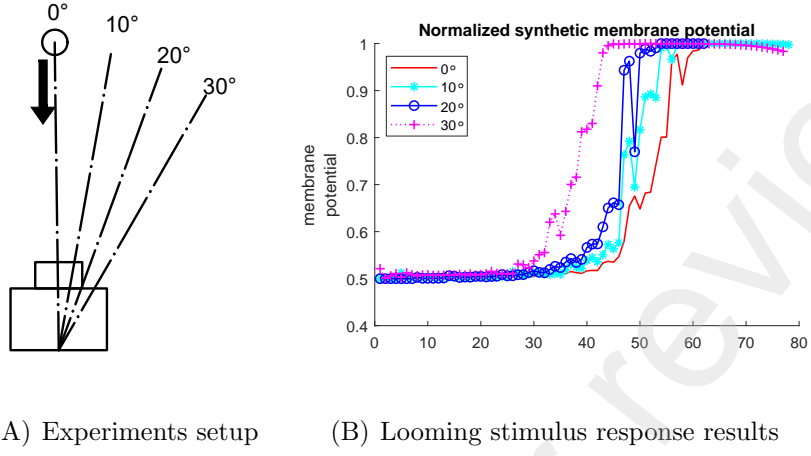


**Fig. 10.** The looming stimulus-response of the O-LGMD in the scenes of an approaching ball with different initial directions. (A) A small ball approaches the camera from four initial directions: the central axis of the camera, off by 10 degrees, 20 degrees, and 30 degrees. (B) The membrane potential curves of O-LGMD when the ball approaches from different initial directions. The results show that within the viewing angle of the camera, no matter from which angle the ball approaches the camera, the corresponding curves of our proposed model are very similar.

Fig. 11(B), at an angle of 0 degrees, where a collision would occur, the output membrane potential of the O-LGMD quickly saturates and remains consistent as the target continues to approach. The peak of O-LGMD membrane potential after normalization is 0.9, 0.7, and less than 0.6 at 10, 20, 30 degrees, respectively. As the globule moves away from the centre of the FOV, the membrane potential drops gradually. These results match the mechanism of real-world neurons: the more significant the angular displacement, the lower the risk of collision, which leads to the lower excitation of the detection neurons.

We also carried out experiments on the scene of a pedestrian approaching camera at night. As illustrated in Fig. 10, the pedestrian is still at a reasonable distance, more than 4 meters from the camera, when the O-LGMD first detected the collision risk at the 144th frame in the blue-theme video. For comparison, LGMD1 did not issue a collision warning signal in the same clip until frame 163, where the pedestrian was less than two meters away from the camera. Figure 11 contains the detection results of another pedestrian

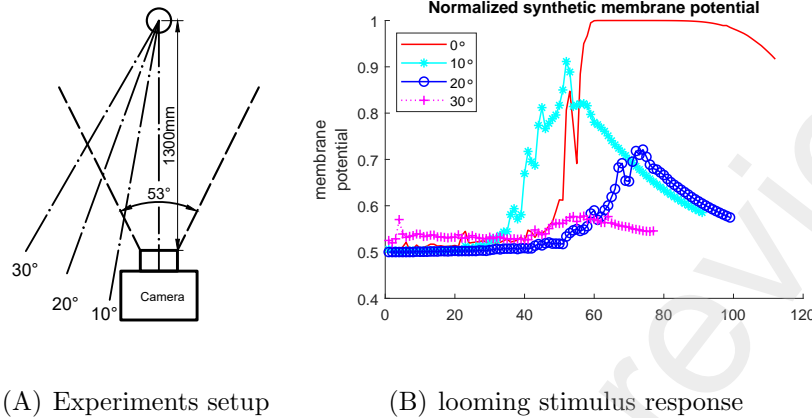


**Fig. 11.** The looming stimulus-response of the O-LGMD in different near-missing angles. (A) The ball starts at the same position and approaches the camera but near misses in different directions, such as 10 degrees, 20 degrees, and 30 degrees to the left of the camera axis. (B) The membrane potential curves of O-LGMD when the ball near misses in different directions. From the result it can be seen when the deflection angle of the ball is less than 10 degrees, the possibility of collision still exists. At this time, the membrane potential of OLGMD will send out a short-term collision warning signal, but as the deviation angle increases, the position where the ball disappears is also a distance away from The camera getting farther and farther away. When the angle is greater than 20 degrees, the membrane potential will always be less than the threshold, and there will be no spike pulse output..

approach scene in the red palette. In this scene, a pedestrian walked toward the camera from about 100 meters. The sizes of the pedestrian first detected in this scene are presented in the images of these two keyframes in the top row. From the bottom two axes are the number of input data, the number on the Y axis indicates at which frame in the video the collision warning was first issued, and the larger number means the later in the timeline. (B) The notched box plot indicates the normalized position where the collision was first detected in videos. The overall average of the O-LGMD model is about 8% ahead of the LGMD1, as shown by curves in the diagram, it can be learned that the O-LGMD first fired warning spikes at the 139th frame, where the pedestrian was about 8 meters away. In the same scene, the LGMD1 model fired its first spikes at frame 157. When detected, the distance between the pedestrian and the camera is around 4 meters. To test the performance of the models in a dynamic circumstance, we allowed the camera moves with a table dolly slider in another group of tests. Fig. 12 shows the test results

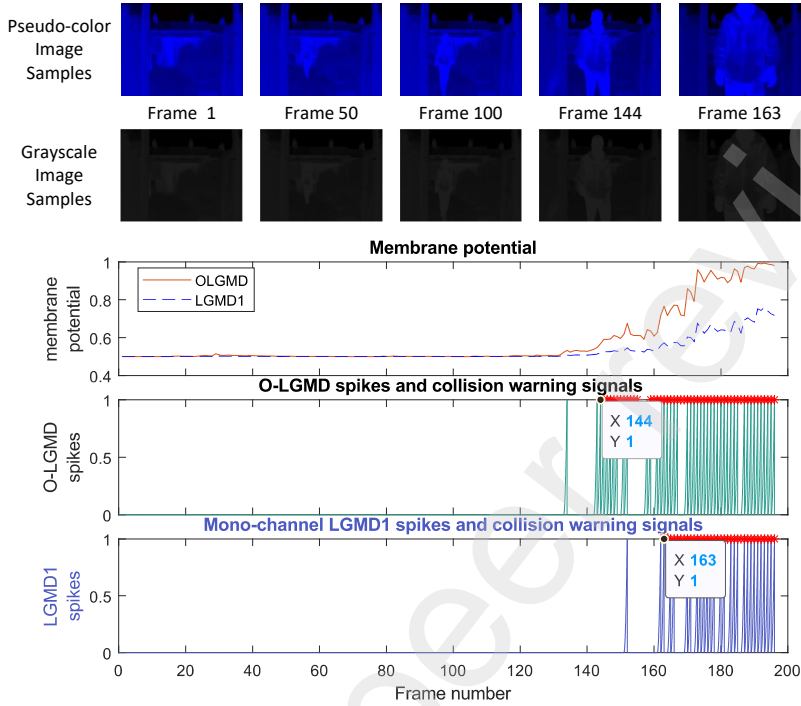


**Fig. 12.** Comparison of the O-LGMD and LGMD1 looming stimulus responses to the pedestrian approaching scene in the blue pseudo-colour palette.

when the camera moves together with a Neewer™ table dolly slider, and there is no obvious collision hazard within the field of view. Although there are slight changes in background colour and salt-and-pepper noise appeared in the test video with the movement of the camera, which caused a slight jitter in the O-LGMD membrane potential, it was eventually suppressed by the group decay mechanism of the LGMD algorithm, so neither model fires the spike and collision warning alerts in this situation. Fig. 12 includes the responses of the O-LGMD and the LGMD1 to a looming stimulus caused by the camera approaching a bottle of 40 degrees Celsius warm water. It can be seen from Fig. 12 that the membrane potential curve of O-LGMD steps up at frame 146 and increases sharply to exceed the threshold at the 190th frame. Since the environment is dark and there is not enough illuminance difference, the detection result of the LGMD1 model in this scene is false negative.

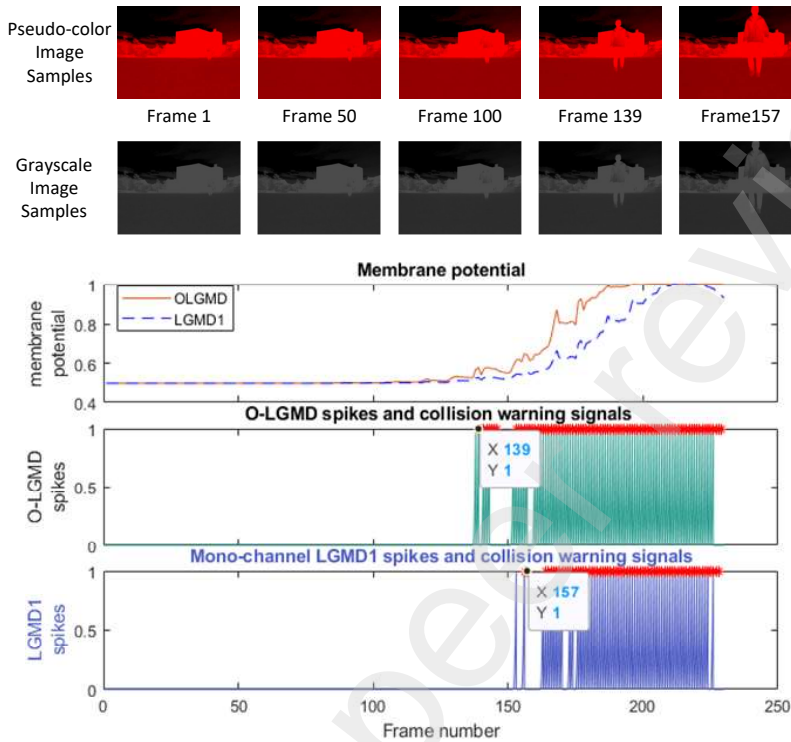


**Fig. 13.** Comparison of the O-LGMD and LGMD1 looming stimulus responses to the pedestrian approaching scene in the red pseudo-colour palette.

Finally, we repeated similar movement stimulus tests in different videos captured by the thermal camera at night. We used two baselines to compare the overall collision detection performance of the models. The first baseline is the frame number when the model issues the first spike, and the second is the ratio of the detected object pixels to the overall image pixels. Fig. 16 shows the statistics of 43 different thermal videos. Both models in each test issue the collision warning signal. Fig. 16(A) is the chart that includes 43 comparisons of the first fire-spike frame number between the O-LGMD (black) and the LGMD1 (red). The red curve is generally above the black one, meaning that the O-LGMD can fire spikes in a more petite frame number, in other words, at an earlier moment, in all the forty-three tests. From the knot box diagram demonstrated in Fig. 16(B), it can conclude that the overall average spike firing time of the O-LGMD model is about 8% ahead of that of

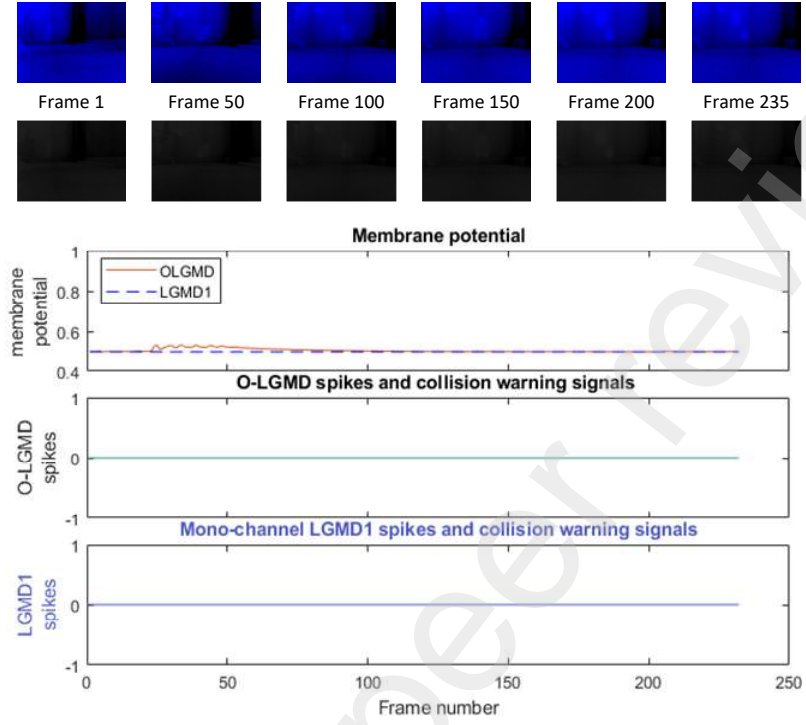


**Fig. 14.** Detection results when the camera moves with a dolly slider, and there are no challenges ahead.

LGMD1.

In addition, we counted the pixels of the impending collision objects in the frame in which the neuron first issued a collision warning during these tests and then further calculated their ratio in the image. As illustrated in Fig. 17, according to the statistical results, when O-LGMD first issued a collision warning, the object accounted for about 20

## 5. Discussion

As described in the above sections, this study has been focusing on enhancing the colour perception ability for collision detection through triple-channel opponent colour LGMD(O-LGMD) neural networks.

Both synthetic and real-world video experiments show that when the detected moving target has noticeable colour differences with the background,

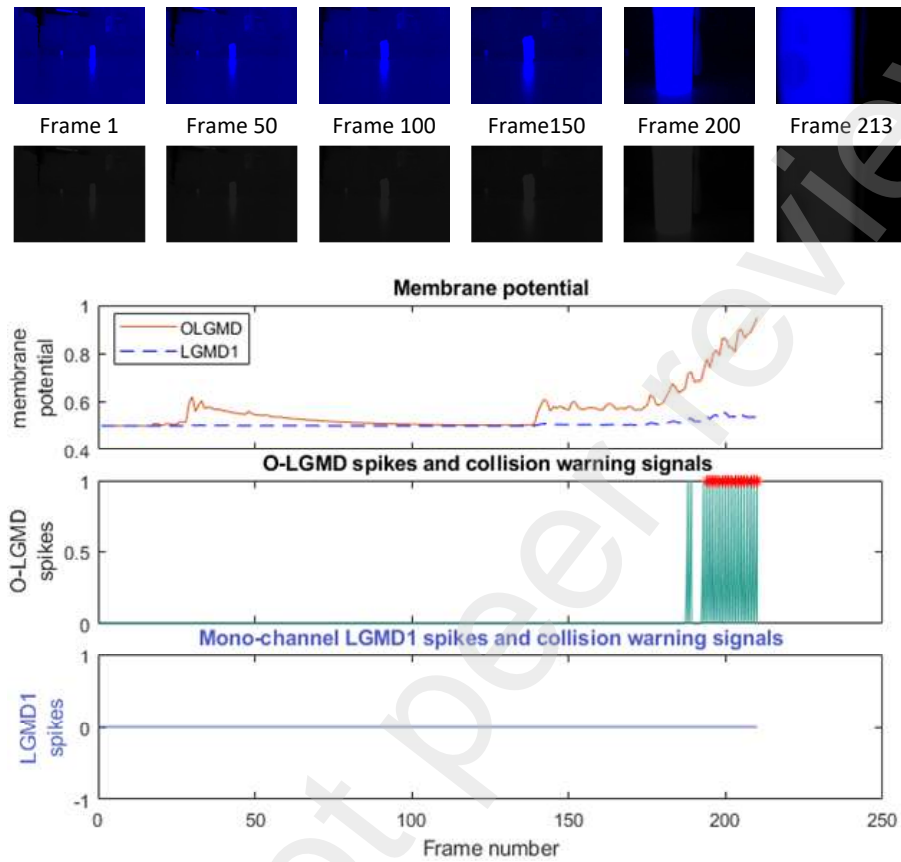


**Fig. 15.** Collision detection results of the camera approaching an object. In this scene, the thermal camera was fixed on a Neewer table dolly slider and moving with it towards a bottle of warm water at 40 degrees Celsius.

but the brightness of the two is similar, our proposed model can effectively detect collision risks, which traditional mono-channel grayscale methods cannot. At the same time, we use a thermal infrared camera instead of an optical camera to collect data. Benefiting from the characteristics of thermal imaging, targets that cannot be distinguished in optics, such as white truck bodies and cement pavement, can be easily distinguished in the thermal radiation image due to their different pseudo colours. Although in the experiments, we found that compared to the single-channel LGMD1, the O-LGMD can always detect moving objects in earlier video frames or when the target size

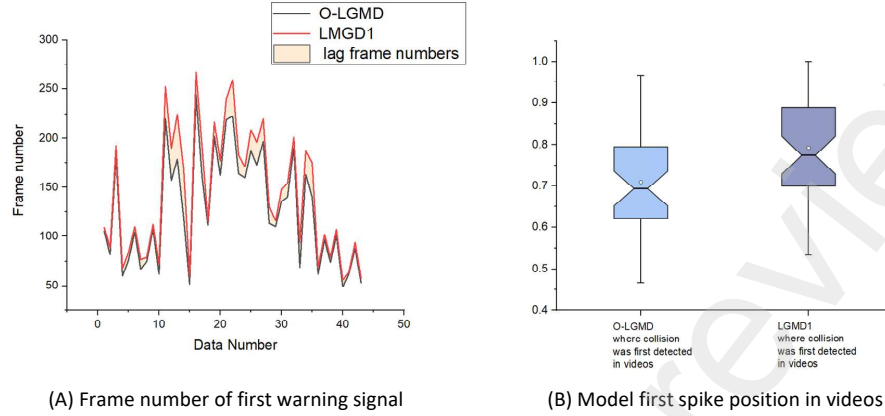


**Fig. 16.** Comparison of the models in early collision detection test between O-LGMD and LGMD1. (A) The horizontal axis is the number of input data, the number on the Y axis indicates at which frame in the video the collision warning was first issued, and the larger number means the later collision detected in the timeline. (B) The notched box plot indicates the normalized position where the collision was first detected in videos. The overall average of the O-LGMD model is about 8% ahead of that of the LGMD1.

is relatively smaller in the field of view. But the complexity of the network structure makes our model run slower on hardware with low performance. Our proposed LGMD model does not apply the ON/OFF mechanism [55, 56], which may enhance the model's ability of colour selectivity. It is worth exploring in the future whether the colour selectivity of the O-LGMD can be better achieved by applying the ON/OFF mechanism.

In nature, the vision of higher animals has evolved towards the direction of colour discrimination. Therefore, we have reason to believe that with the improvement of hardware, colour resolution ability will also play an important role in collision detection.

## 6. Conclusion

In this work, we proposed an O-LGMD neural network with three opponent colour processing pathways for collision detection at nighttime with thermal images. Like the structure of the lateral geniculate nucleus in the primate thalamus, the proposed network has one channel for the luminance signal and two for the opponent colour information. Experiments indicated that

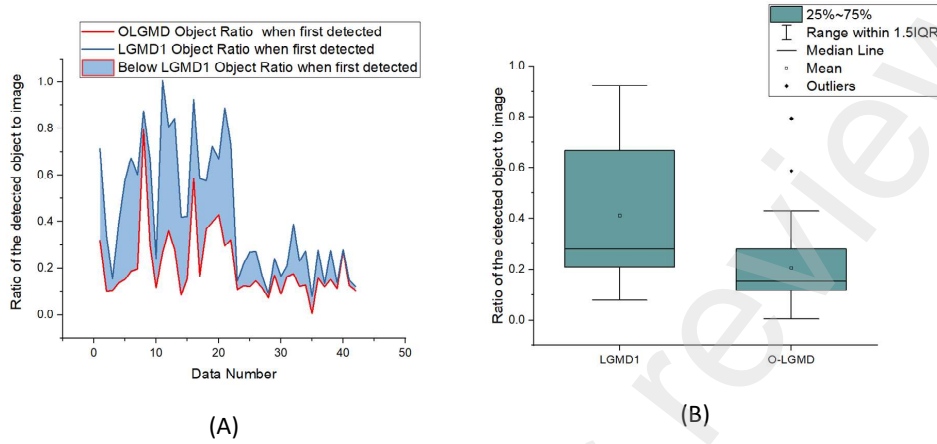


**Fig. 17.** The ratio of the object to the image when the object was first detected. (A) Curves present the proportional relationship between the pixels of the object and the total pixels of the image when the neural network first fires a collision warning spike in 43 different false-colour thermal infrared data. (B) The result plotted in a box plot, by comparing the mean values of the two, it can be known that the size of the object when the O-LGMD detects a collision is about 20% smaller than that of the LGMD1.

the O-LGMD network had utilized the advantages of opponent colour processing methods well to distinguish colours that are ambiguous in grayscale images effectively. Systematic studies have also demonstrated that the O-LGMD model improves the sensitivity of collision recognition in specific infrared pseudo-colour palettes, such as monochromatic themes in blue or red. This feature supports the O-LGMD to detect collision risks earlier than the conventional LGMD1 algorithm in the dark. In the future, we will combine a thermal camera with an optical colour camera to investigate more efficient collision detection methodologies in complex dim light environments.

## 7. Acknowledgement

This research was supported by the EU HORIZON 2020 project UL-TRACEPT (778062) and the National Natural Science Foundation of China project (62073091).

## References

- [1] F. C. Rind, D. Bramwell, Neural network based on the input organization of an identified neuron signaling impending collision, *Journal of neurophysiology* 75 (3) (1996) 967–985.
- [2] S. Yue, F. C. Rind, Collision detection in complex dynamic scenes using an lgmd-based visual neural network with feature enhancement, *IEEE transactions on neural networks* 17 (3) (2006) 705–716.
- [3] D. Jayachandran, A. Oberoi, A. Sebastian, T. H. Choudhury, B. Shankar, J. M. Redwing, S. Das, A low-power biomimetic collision detector based on an in-memory molybdenum disulfide photodetector, *Nature Electronics* 3 (10) (2020) 646–655.
- [4] J. Zhao, H. Wang, N. Bellotto, C. Hu, J. Peng, S. Yue, Enhancing lgmd's looming selectivity for UAV with spatial-temporal distributed presynaptic connections, *IEEE Transactions on Neural Networks and Learning Systems* (2021).
- [5] J. Zhao, X. Ma, Q. Fu, C. Hu, S. Yue, An lgmd based competitive collision avoidance strategy for UAV, in: IFIP International Conference on Artificial Intelligence Applications and Innovations, Springer, 2019, pp. 80–91.
- [6] J. Zhao, C. Hu, C. Zhang, Z. Wang, S. Yue, A bio-inspired collision detector for small quadcopter, in: 2018 International Joint Conference on Neural Networks (IJCNN), IEEE, 2018, pp. 1–7.
- [7] L. He, N. Aouf, J. F. Whidborne, B. Song, Integrated moment-based lgmd and deep reinforcement learning for uav obstacle avoidance, in: 2020 IEEE International Conference on Robotics and Automation (ICRA), IEEE, 2020, pp. 7491–7497.
- [8] L. Salt, G. Indiveri, Y. Sandamirskaya, Obstacle avoidance with LGMD neuron: towards a neuromorphic uav implementation, in: 2017 IEEE International Symposium on Circuits and Systems (ISCAS), IEEE, 2017, pp. 1–4.
- [9] M. Blanchard, F. C. Rind, P. F. Verschure, Collision avoidance using a model of the locust LGMD neuron, *Robotics and Autonomous Systems* 30 (1-2) (2000) 17–38.

- [10] Q. Fu, C. Hu, T. Liu, S. Yue, Collision selective LGMDs neuron models research benefits from a vision-based autonomous micro robot, in: 2017 IEEE/RSJ International Conference on Intelligent Robots and Systems (IROS), IEEE, 2017, pp. 3996–4002.
- [11] C. Hu, F. Arvin, C. Xiong, S. Yue, Bio-inspired embedded vision system for autonomous micro-robots: The lgmd case, *IEEE Transactions on Cognitive and Developmental Systems* 9 (3) (2017) 241–254.
- [12] S. Yue, F. C. Rind, A collision detection system for a mobile robot inspired by the locust visual system, in: Proceedings of the 2005 IEEE International Conference on Robotics and Automation, IEEE, 2005, pp. 3832–3837.
- [13] Q. Fu, N. Bellotto, H. Wang, F. Claire Rind, H. Wang, S. Yue, A visual neural network for robust collision perception in vehicle driving scenarios, in: IFIP International Conference on Artificial Intelligence Applications and Innovations, Springer, 2019, pp. 67–79.
- [14] M. Hartbauer, Simplified bionic solutions: a simple bio-inspired vehicle collision detection system, *Bioinspiration & biomimetics* 12 (2) (2017) 026007.
- [15] S. Yue, F. C. Rind, Visual motion pattern extraction and fusion for collision detection in complex dynamic scenes, *Computer Vision and Image Understanding* 104 (1) (2006) 48–60.
- [16] M. Bratkova, S. Boulos, P. Shirley, oRGB: a practical opponent color space for computer graphics, *IEEE computer graphics and applications* 29 (1) (2008) 42–55.
- [17] D. M. Dacey, Parallel pathways for spectral coding in primate retina, *Annual review of neuroscience* 23 (1) (2000) 743–775.
- [18] U. Grünert, P. R. Martin, Cell types and cell circuits in human and non-human primate retina, *Progress in retinal and eye research* 78 (2020) 100844.
- [19] S. H. Hendry, R. C. Reid, et al., The koniocellular pathway in primate vision, *Annual review of neuroscience* 23 (1) (2000) 127–153.

- [20] M. O'shea, C. Rowell, The neuronal basis of a sensory analyser, the acridid movement detector system. ii. response decrement, convergence, and the nature of the excitatory afferents to the fan-like dendrites of the lgmd, *Journal of Experimental Biology* 65 (2) (1976) 289–308.
- [21] M. O'Shea, J. Williams, The anatomy and output connection of a locust visual interneurone; the lobular giant movement detector (lgmd) neurone, *Journal of comparative physiology* 91 (3) (1974) 257–266.
- [22] N. Hatsopoulos, F. Gabbiani, G. Laurent, Elementary computation of object approach by a wide-field visual neuron, *Science* 270 (5238) (1995) 1000–1003.
- [23] F. Gabbiani, H. G. Krapp, G. Laurent, Computation of object approach by a wide-field, motion-sensitive neuron, *Journal of Neuroscience* 19 (3) (1999) 1122–1141.
- [24] F. Gabbiani, C. Mo, G. Laurent, Invariance of angular threshold computation in a wide-field looming-sensitive neuron, *Journal of Neuroscience* 21 (1) (2001) 314–329.
- [25] H. Meng, K. Appiah, S. Yue, A. Hunter, M. Hobden, N. Priestley, P. Hobden, C. Pettit, A modified model for the lobula giant movement detector and its fpga implementation, *Computer vision and image understanding* 114 (11) (2010) 1238–1247.
- [26] Q. Fu, S. Yue, Modelling lgmd2 visual neuron system, in: 2015 IEEE 25th International Workshop on Machine Learning for Signal Processing (MLSP), IEEE, 2015, pp. 1–6.
- [27] F. Lei, Z. Peng, V. Cutsuridis, M. Liu, Y. Zhang, S. Yue, Competition between on and off neural pathways enhancing collision selectivity, in: 2020 International Joint Conference on Neural Networks (IJCNN), IEEE, 2020, pp. 1–8.
- [28] F. Lei, Z. Peng, M. Liu, J. Peng, V. Cutsuridis, S. Yue, A robust visual system for looming cue detection against translating motion, *IEEE Transactions on Neural Networks and Learning Systems* (2022).

- [29] M. Hua, Q. Fu, W. Duan, S. Yue, Investigating refractoriness in collision perception neuronal model, in: 2021 International Joint Conference on Neural Networks (IJCNN), IEEE, 2021, pp. 1–8.
- [30] G. Zhang, C. Zhang, S. Yue, Lgmd and dsns neural networks integration for collision predication, in: 2016 International Joint Conference on Neural Networks (IJCNN), IEEE, 2016, pp. 1174–1179.
- [31] Q. Fu, C. Hu, P. Liu, S. Yue, Synthetic neural vision system design for motion pattern recognition in dynamic robot scenes, arXiv preprint arXiv:1904.07180 (2019).
- [32] C. Hu, C. Xiong, J. Peng, S. Yue, Coping with multiple visual motion cues under extremely constrained computation power of micro autonomous robots, IEEE Access 8 (2020) 159050–159066.
- [33] B. B. Lee, The evolution of concepts of color vision, Neurociencias 4 (4) (2008) 209.
- [34] R. Haidar, Thomas young and the wave theory of light, PDF). Bibnum. Retrieved 5 (2016).
- [35] H. Helmholtz, The young–helmholtz theory of color vision, Dennis, Wayne 1948 (1860) 199.
- [36] E. Hering, Opponent-process theory, Expanded by Solomon (1878).
- [37] R. L. De Valois, K. K. De Valois, A multi-stage color model, Vision research 33 (8) (1993) 1053–1065.
- [38] I. P. Howard, The helmholtz–hering debate in retrospect (1999).
- [39] F. Zhang, K. Kurokawa, A. Lassoued, J. A. Crowell, D. T. Miller, Cone photoreceptor classification in the living human eye from photostimulation-induced phase dynamics, Proceedings of the National Academy of Sciences 116 (16) (2019) 7951–7956.
- [40] J. Schnapf, T. Kraft, D. Baylor, Spectral sensitivity of human cone photoreceptors, Nature 325 (6103) (1987) 439–441.

- [41] F. De Monasterio, P. Gouras, D. Tolhurst, Trichromatic colour opponency in ganglion cells of the rhesus monkey retina., *The Journal of Physiology* 251 (1) (1975) 197–216.
- [42] N. A. Ibraheem, M. M. Hasan, R. Z. Khan, P. K. Mishra, Understanding color models: a review, *ARPN Journal of science and technology* 2 (3) (2012) 265–275.
- [43] L. Dong, W. Zhang, W. Xu, Underwater image enhancement via integrated RGB and LAB color models, *Signal Processing: Image Communication* 104 (2022) 116684.
- [44] F. Yan, N. Li, K. Hirota, QHSL: A quantum hue, saturation, and lightness color model, *Information Sciences* 577 (2021) 196–213.
- [45] M. R. Luo, M.-C. Lo, W.-G. Kuo, The LLAB (l: c) colour model, *Color Research & Application* 21 (6) (1996) 412–429.
- [46] T. Fu, X. Zhao, L. Chen, W.-S. Wu, Q. Zhao, X.-L. Wang, D.-M. Guo, Y.-Z. Wang, Bioinspired color changing molecular sensor toward early fire detection based on transformation of phthalonitrile to phthalocyanine, *Advanced Functional Materials* 29 (8) (2019) 1806586.
- [47] M. Hashemzadeh, A. Zademehdhi, Fire detection for video surveillance applications using ica k-medoids-based color model and efficient spatio-temporal visual features, *Expert Systems with Applications* 130 (2019) 60–78.
- [48] K. Nikolskaia, N. Ezhova, A. Sinkov, M. Medvedev, Skin detection technique based on hsv color model and slic segmentation method, in: *Proceedings of the 4th Ural Workshop on Parallel, Distributed, and Cloud Computing for Young Scientists, Ural-PDC 2018. CEUR Workshop Proceedings*, Vol. 2281, 2018, pp. 123–135.
- [49] J. Deng, Analysis and recognition based on citrus color grading model considering computer vision technology, *Advances in Multimedia* 2021 (2021).
- [50] A. C. Smith, H. M. Buchanan-Smith, A. K. Surridge, D. Osorio, N. I. Mundy, The effect of colour vision status on the detection and selection

of fruits by tamarins (*saguinus* spp.), *Journal of Experimental Biology* 206 (18) (2003) 3159–3165.

- [51] P. Ganesan, V. Rajini, R. I. Rajkumar, Segmentation and edge detection of color images using cielab color space and edge detectors, *INTERACT-2010* (2010) 393–397.
- [52] L. Peihua, A clustering-based color model and integral images for fast object tracking, *Signal Processing: Image Communication* 21 (8) (2006) 676–687.
- [53] G.-J. Jang, I.-S. Kweon, Robust object tracking using an adaptive color model, in: *Proceedings 2001 ICRA. IEEE International Conference on Robotics and Automation (Cat. No. 01CH37164)*, Vol. 2, IEEE, 2001, pp. 1677–1682.
- [54] V. J. Tsai, A comparative study on shadow compensation of color aerial images in invariant color models, *IEEE transactions on geoscience and remote sensing* 44 (6) (2006) 1661–1671.
- [55] E. H. Doeven, E. M. Zammit, G. J. Barbante, P. S. Francis, N. W. Barnett, C. F. Hogan, A potential-controlled switch on/off mechanism for selective excitation in mixed electrochemiluminescent systems, *Chemical Science* 4 (3) (2013) 977–982.
- [56] Q. Fu, C. Hu, J. Peng, F. C. Rind, S. Yue, A robust collision perception visual neural network with specific selectivity to darker objects, *IEEE transactions on cybernetics* 50 (12) (2019) 5074–5088.